

# Interacting Anisotropic Dirac Fermions in Strained Graphene and Related Systems

Anand Sharma,<sup>1</sup> Valeri N. Kotov,<sup>1</sup> and Antonio H. Castro Neto<sup>2,3</sup>

<sup>1</sup>*Department of Physics, University of Vermont, 82 University Place, Burlington, Vermont 05405, USA*

<sup>2</sup>*Department of Physics, Boston University, 590 Commonwealth Avenue, Boston, Massachusetts 02215, USA*

<sup>3</sup>*Graphene Research Centre and Department of Physics,  
National University of Singapore, 2 Science Drive 3, Singapore 117542*

(Dated: March 8, 2013)

We study the role of long-range electron-electron interactions in a system of two-dimensional anisotropic Dirac fermions, which naturally appear in uniaxially strained graphene, graphene in external potentials, some strongly anisotropic topological insulators, and engineered anisotropic graphene structures. We find that while for small interactions and anisotropy the system restores the conventional isotropic Dirac liquid behavior, strong enough anisotropy can lead to the formation of a quasi-one dimensional electronic phase with dominant charge order (anisotropic excitonic insulator).

Since the isolation of graphene [1], a two dimensional (2D) allotrope of carbon, there has been substantial theoretical and experimental effort to understand and utilize its remarkable mechanical [2], thermal [3], electronic [4] and transport [5] properties. The charge carriers in a pristine graphene sheet move on a honeycomb lattice (Fig. 1(a)) as if they were massless relativistic particles. The physical properties at low energies are governed by the Dirac Hamiltonian resulting in a linear dispersion and isotropic cones (with circular cross section) near the Dirac points (Fig. 1(b)). Mechanical deformations, such as uniaxial strain for example along the armchair direction (Fig. 1(c)), can lead to anisotropic dispersion with the formation of elliptical Dirac cones (Fig. 1(d)) [6]. Within the tight-binding and *ab initio* schemes, the anisotropic Dirac dispersion is found for weak to moderate uniaxial strain in any direction, while for large strain the electronic structure becomes very different along the armchair and zig-zag directions, ultimately leading to cone merger and gap formation in the latter case [6]. It has also been shown that anisotropic Dirac cones can be formed by applying an external periodic potential [7] on graphene. Such changes of the band structure can provide exciting possibilities for “strain engineering,” i.e. manipulation of graphene’s electronic, optical, etc. properties by applying lattice deformations or potentials [8]. Strongly anisotropic Dirac cones can also appear in certain topological insulators [9], and, in a recent development, highly tunable honeycomb optical lattices and molecular graphene systems have been created [10], providing a possible route towards exploring various anisotropic phases.

The subject of the present work is the interplay between Dirac fermion anisotropy and electron interactions. It is known that near the Dirac point, close to charge neutrality, unscreened long-range electron-electron interactions in isotropic graphene can manifest themselves in a variety of ways [11]; perhaps most spectacularly interactions lead to logarithmic renormalization of the electron spectrum leading to reshaping of the Dirac cones (velocity increase), observed in undeformed suspended

graphene [12]. Previously anisotropic Dirac fermions have been studied in QED<sub>3</sub>-type models, relevant for the cuprate superconductors, where the fermion anisotropy was found to be irrelevant in renormalization group (RG) sense [13], i.e. the systems flows towards the isotropic limit. This behavior can be reversed, i.e. the anisotropy increases, if the fermions couple to a nematic order parameter, as suggested for the cuprates [14].

In this work we show that in graphene-based anisotropic Dirac systems, as they arise in modified (i.e. strained, or artificially engineered) graphene, a rich variety of behavior can take place due to electron-electron interactions. Within the RG approach we find that for small interactions and anisotropy, the system flows towards the conventional isotropic fixed point. However the anisotropy also favors a transition towards an excitonic insulator (whose existence is well established in the isotropic case [15]), making this phase accessible for much smaller interactions compared to isotropic

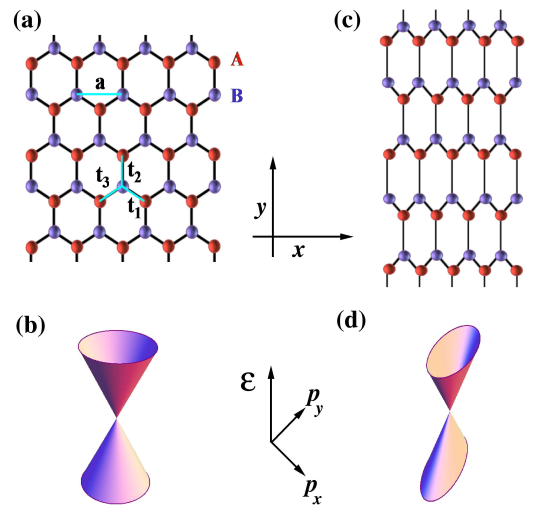


FIG. 1: (Color online) Honeycomb lattice for (a) undeformed and (c) uniaxially deformed graphene along the  $y$  (armchair) direction. The corresponding isotropic (b) and anisotropic (d) Dirac cones are shown.

graphene. We show that provided the anisotropy is large enough, a quasi one-dimensional phase with dominant charge density wave order (anisotropic excitonic insulator) can form even for small interactions. Thus strongly anisotropic graphene-based systems can relatively easily experience interaction-driven transitions towards novel electronic phases, providing a promising avenue for exploration of unconventional many-body physics.

*Dispersion anisotropy.* We consider, for definitiveness, graphene under uniaxial strain. Without interactions, the Hamiltonian is [6]:  $\hat{H}_0 = v_x p_x \hat{\sigma}_x + v_y p_y \hat{\sigma}_y$ , where  $\hat{\sigma}_x, \hat{\sigma}_y$  are the usual  $(2 \times 2)$  Pauli matrices. Here  $v_x = t_2 a_x \sqrt{4\eta^2 - 1}$ ,  $v_y = t_2 a_y$  are the velocities along the  $x$ - and  $y$ - direction respectively.;  $\eta = \frac{t_1}{t_2} = \frac{t_3}{t_2}$ ,  $a_x = a/2$  and  $a_y = \frac{\sqrt{3}}{2}a$ , with  $a \approx \sqrt{3} \times 1.42 \text{ \AA}$ , as shown in Fig. 1(a). The electronic dispersion, as shown in Fig. 1(d) is:

$$\varepsilon(\mathbf{p}) = \pm \sqrt{v_x^2 p_x^2 + v_y^2 p_y^2}, \quad \frac{v_y}{v_x} \equiv 1 + \delta. \quad (1)$$

and we have also defined, and will use from now on the anisotropy parameter  $\delta$ . We will explore the range  $-1 \leq \delta \leq 0$ , i.e.  $0 \leq v_y/v_x \leq 1$ , which in the notation of Fig. 1(c) would imply strain in the armchair ( $y$ ) direction, with  $v_y < v_x$ . Clearly  $\delta = 0$  corresponds to the isotropic case, while  $\delta = -1$  is the limit of decoupled chains. Strain in the zig-zag ( $x$ ) direction can be easily described by the same parameter range with appropriate relabeling of the axes. The anisotropy parameter  $\delta$  is proportional to the strain [6]. From now on we use the effective anisotropic dispersion (1) which, as mentioned earlier, is relevant to a variety of graphene related systems, and is not necessarily due to strain.

*Electron-electron interactions and anisotropy.* The bare long-range Coulomb potential in graphene is given by  $V(\mathbf{p}) = \frac{2\pi e^2}{\kappa|\mathbf{p}|}$ , where  $\kappa$  is the appropriate dielectric constant. We consider graphene at charge neutrality where the chemical potential  $\mu = 0$  and  $V(\mathbf{p})$  is unscreened. The interaction effects can be incorporated into the self-energy  $\hat{\Sigma}(\mathbf{p}, \varepsilon)$ , so that the fermion Green's function (GF) is given by:  $\hat{G}^{-1}(\mathbf{p}, \varepsilon) = \varepsilon \hat{\sigma}_0 - v_x p_x \hat{\sigma}_x - v_y p_y \hat{\sigma}_y - \hat{\Sigma}(\mathbf{p}, \varepsilon)$ , where  $\hat{\sigma}_0$  is the identity matrix. We work in the two-loop approximation, i.e.  $\hat{\Sigma}(\mathbf{p}, \varepsilon) = \hat{\Sigma}^{(2)}(\mathbf{p}, \varepsilon) = i \sum_{\mathbf{q}} \int_{-\infty}^{\infty} \frac{d\omega}{2\pi} V^{(2)}(\mathbf{p} - \mathbf{q}, \varepsilon - \omega) \hat{G}^{(0)}(\mathbf{q}, \omega)$  with the effective interaction  $V^{(2)}(\mathbf{q}, \omega) = V(\mathbf{q}, \omega) + (V(\mathbf{q}, \omega))^2 \Pi(\mathbf{q}, \omega)$ , and  $\hat{G}^{(0)}$  is the free GF. The physical reasons behind the use of the two-loop approximation will be discussed later and vertex corrections are neglected as their effect is small, similarly to the case of isotropic graphene [16]. The dynamical polarization bubble for anisotropic Dirac fermions is easily evaluated to be:

$$\Pi(\mathbf{q}, \omega) = -\frac{N}{16v_x v_y} \frac{v_x^2 q_x^2 + v_y^2 q_y^2}{\sqrt{v_x^2 q_x^2 + v_y^2 q_y^2 - \omega^2}}, \quad (2)$$

with  $N$  being the number of fermion flavors ( $N = 4$  for graphene.) Using the standard decomposition  $\hat{\Sigma}^{(2)} = \varepsilon \hat{\sigma}_0 \Sigma_0 + v_x p_x \hat{\sigma}_x \Sigma_x + v_y p_y \hat{\sigma}_y \Sigma_y$  we obtain the dressed Green's function [11]:

$$\hat{G}(\mathbf{p}, \varepsilon) = \frac{Z(l)}{\varepsilon \hat{\sigma}_0 - v_x(l) p_x \hat{\sigma}_x - v_y(l) p_y \hat{\sigma}_y} \quad (3)$$

where  $v_x(l)/v_x = Z(l)(1 + \Sigma_x(l))$ ,  $v_y(l)/v_y = Z(l)(1 + \Sigma_y(l))$ , and the quasiparticle residue is  $Z(l) = (1 - \Sigma_0(l))^{-1} \approx 1 + \Sigma_0(l)$ . At low energies,  $|\mathbf{p}| \equiv p \rightarrow 0$ , all quantities diverge logarithmically in terms of the parameter  $l = \ln(\Lambda/p)$ , where  $\Lambda$  is the ultraviolet cutoff. We obtain by direct calculation the divergent contributions:

$$\Sigma_0(l) = -\alpha_x^2 \frac{N}{24(1+\delta)} \ln(\Lambda/p), \quad (4)$$

$$\Sigma_{x,y}(l) = \left\{ \frac{1}{2} \alpha_x I_{1,3} - \frac{N}{24(1+\delta)} \alpha_x^2 (3 - 4I_{2,4}) \right\} \ln(\Lambda/p). \quad (5)$$

Here  $I_i = I_i(\delta)$ ,  $i = 1, 2, 3, 4$  are evaluated as follows. Define  $C(\theta, \delta) = \cos^2 \theta + (1 + \delta)^2 \sin^2 \theta$ , then we have  $I_n(\delta) = \frac{1}{2\pi} \int_0^{2\pi} \frac{\cos^2 \theta d\theta}{[C(\theta, \delta)]^{n/2}}$ , for  $n = 1, 2$ , and  $I_3(\delta) = \frac{1}{2\pi} \int_0^{2\pi} \frac{\sin^2 \theta d\theta}{\sqrt{C(\theta, \delta)}}$ ,  $I_4(\delta) = \frac{1}{2\pi} \int_0^{2\pi} \frac{(1+\delta)^2 \sin^2 \theta d\theta}{C(\theta, \delta)}$ .

Since  $1 + \delta = v_y/v_x \leq 1$ , it is convenient to define the dimensionless Coulomb interaction coupling  $\alpha_x = \frac{e^2}{\kappa v_x}$ . From Eqs. (4,5) we obtain the RG equations for  $\alpha_x(l)$  and the anisotropy  $\delta(l)$ :

$$\frac{d\alpha_x}{dl} = -\frac{\alpha_x^2}{2} I_1(\delta) + \frac{N\alpha_x^3}{6(1+\delta)} (1 - I_2(\delta)) \quad (6)$$

$$\frac{d\delta}{dl} = (1 + \delta) \frac{\alpha_x}{2} (I_3(\delta) - I_1(\delta)) - \frac{N\alpha_x^2}{6} (I_2(\delta) - I_4(\delta)) \quad (7)$$

We assume  $1 + \delta \geq 0$ . It is also instructive to write these equations in the small anisotropy limit,  $\delta \ll 1$ :

$$\frac{d\alpha_x}{dl} = -\frac{\alpha_x^2}{4} \left\{ 1 - \frac{\delta}{4} + \frac{\delta^2}{16} \right\} + \frac{\alpha_x^3}{3} \left\{ 1 - \frac{\delta}{2} + \frac{\delta^2}{4} \right\} \quad (8)$$

$$\frac{d\delta}{dl} = -\frac{\delta\alpha_x}{8} (1 - \delta^2) + \frac{\delta\alpha_x^2}{3} \left( 1 - \frac{\delta}{2} \right) \quad (9)$$

In the opposite limit of strong anisotropy,  $\delta \approx -1$ , we obtain:

$$\frac{d\alpha_x}{dl} = -\frac{\alpha_x^2}{\pi} + \frac{2\alpha_x^3}{3}, \quad \frac{d\delta}{dl} = (1 + \delta) \frac{\alpha_x}{4} \ln \left( \frac{4}{1 + \delta} \right) - \frac{2\alpha_x^2}{3} \quad (10)$$

*RG results: possible electronic phases.* The numerical solution of the RG equations, Eq. (6) and (7), with  $N = 4$ , leads us to the RG flow in Fig. 2 which is the main

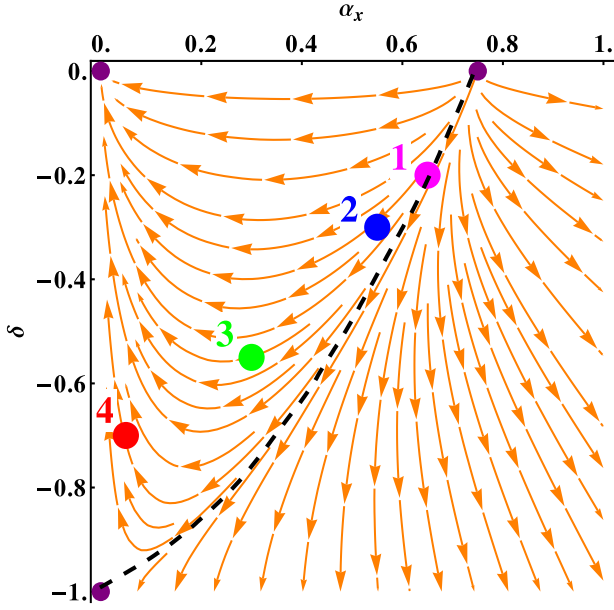


FIG. 2: (Color online) RG flow in the plane  $(\alpha_x, \delta)$ , in terms of the interaction  $\alpha_x = \frac{e^2}{\kappa v_x}$  and the anisotropy,  $\delta \equiv \frac{v_y - v_x}{v_x}$ . There is a stable fixed point at  $(0, 0)$  and unstable fixed points at  $(0, -1)$  and  $(3/4, 0)$ . The broken line  $\alpha_{x,c}(\delta)$  separates a region of  $\alpha_x$  flowing to zero, for  $\alpha_x < \alpha_{x,c}(\delta)$ , and the region  $\alpha_x > \alpha_{x,c}(\delta)$  where  $\alpha_x$  either increases or flows towards a finite value. The evolution of the couplings at the four points labeled by numbers are further shown in Fig. 3.

result of this work. The arrows represent the variations of the couplings as the RG parameter  $l = \ln(\Lambda/p)$  varies from 0 towards  $\infty$  (low-energy limit).

First, notice that at zero anisotropy ( $\delta = 0$ ) there is an unstable fixed point at  $\alpha_c = 3/4$ ; the flow towards strong coupling at  $\alpha_x > \alpha_c$  corresponds to an excitonic insulator [15], i.e. a system with a finite gap in the spectrum (see later discussion.) Within the perturbative RG scheme this fixed point arises from the competition between the one and two loop contributions [16], as is clear from Eqs. (8),(9). Of course one cannot hope to reliably obtain the exact value of  $\alpha_c$  at intermediate coupling, but the very existence of  $\alpha_c$  has been well established by different methods [15], with the result  $\alpha_c \approx 1.1$ . Thus we use the two-loop result in  $\alpha_x$  and then take into account the anisotropy exactly. The dashed line  $\alpha_{x,c}(\delta)$  in Fig. 2 separates a phase with a flow towards the stable fixed point at  $\alpha_x = 0, \delta = 0$  and a region with a flow towards large (diverging) or finite  $\alpha_x$ . We will show shortly that the latter case,  $\alpha_x > \alpha_{x,c}(\delta)$ , is indeed characterized by a divergent susceptibility towards excitonic insulator. For small  $\delta$  we find that  $\alpha_x(l)$  becomes large beyond the modified excitonic transition line, which can be calculated from Eq. (8) to be:  $\alpha_{x,c}(\delta) \approx (3/4)(1 - |\delta|/4)$ . Thus the anisotropy shifts the excitonic transition to smaller coupling ( $\alpha_{x,c}(\delta)$  decreases as  $|\delta|$  increases).

Even below the excitonic transition line  $\alpha_x < \alpha_{x,c}(\delta)$

the anisotropy flow of  $\delta(l)$  towards zero can be very slow and non-monotonic, as shown in Fig. 3. This is especially true for initial values close to the excitonic line. Notice that  $\delta(l)$  in fact increases for small  $l$  up to  $l = 10 - 20$ . Therefore such a signature can be easily observed for graphene at finite Fermi energy (or temperature). For example if at  $T = 0$  the Fermi energy is  $\mu \approx 0.2$  meV we have to stop the RG flow at  $l^* = \ln(v_x \Lambda / \mu) \approx 10$  (taking  $v_x \Lambda = 5$  eV), resulting in an increase of  $\delta$  up to a factor of 2 (or more) depending on the proximity to the excitonic line (curves 1,2 in Fig. 3).

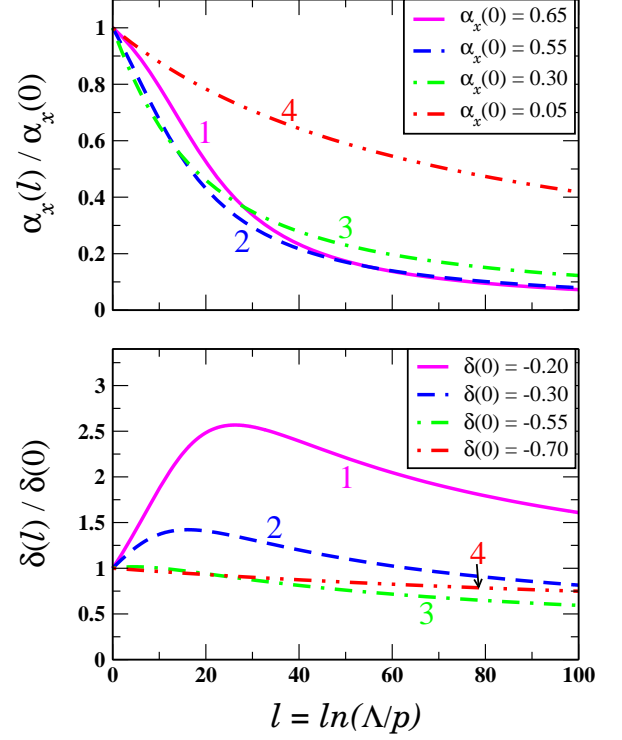


FIG. 3: (Color online) Evolution of the couplings  $\alpha_x(l)$  (upper panel) and  $\delta(l)$  (lower panel) for initial values corresponding to the four numbered points from Fig. 2.

For  $\alpha_x > \alpha_{x,c}(\delta)$  the region of moderate anisotropy and relatively weak coupling,  $0.4 \lesssim |\delta|$ ,  $\alpha_x \lesssim 0.6$ , below the dashed line (Fig. 2) deserves special attention. Here the flow is towards finite  $\alpha_x$  and  $\delta \rightarrow -1$ , i.e. the one-dimensional (1D) limit. From Eq. (10), valid close to the 1D line, we can see that  $\alpha_x^* = 3/(2\pi) = 0.48$  separates regimes where  $\alpha_x$  either experiences (relatively small) decrease, or increases under RG flow as the system approaches the 1D limit. Flow of  $|\delta|$  beyond 1 is not allowed since it reverses the sign of the velocity.

In order to characterize the nature of the phase for  $\alpha_x > \alpha_{x,c}(\delta)$ , we introduce in the Hamiltonian infinitesimal couplings  $\Delta_\mu$  to potential order parameters (in the particle-hole channel):  $\Delta_\mu \sum_{\mathbf{k}} \Psi_{\mathbf{k}}^\dagger \hat{\sigma}_\mu \Psi_{\mathbf{k}}$ ,  $\mu = x, y, z$ . We then compute the interaction corrections to the corresponding vertex functions  $\Gamma_\mu = \Delta_\mu(1 + \chi_\mu \ln(\Lambda/p))$  and

find the susceptibilities:

$$\chi_z = \frac{\alpha_x}{2} J_z(\delta), \quad \chi_{x,y} = \chi_z - \frac{\alpha_x}{2} J_{x,y}(\delta). \quad (11)$$

Here  $J_z(\delta) = \frac{1}{2\pi} \int_0^{2\pi} \frac{d\theta}{\sqrt{C(\theta,\delta)}}$ ,  $J_x(\delta) = \frac{1}{2\pi} \int_0^{2\pi} \frac{\cos^2 \theta d\theta}{[C(\theta,\delta)]^{3/2}}$ ,  $J_y(\delta) = \frac{1}{2\pi} \int_0^{2\pi} \frac{(1+\delta)^2 \sin^2 \theta d\theta}{[C(\theta,\delta)]^{3/2}}$ , and  $C(\theta,\delta) = \cos^2 \theta + (1+\delta)^2 \sin^2 \theta$ . The quantities  $\chi_\mu(l)$  depend on the scale  $l$  via the RG running of  $\alpha_x(l), \delta(l)$ . Divergence of  $\chi_\mu(l)$  at  $l = l^*$  signals spontaneous breakdown of symmetry in the corresponding channel [17]. We have found that  $\chi_z(l)$  is the fastest divergent susceptibility throughout the region  $\alpha_x > \alpha_{x,c}(\delta)$ , and therefore the system is an excitonic insulator with an order parameter  $\langle \Psi^\dagger \hat{\sigma}_z \Psi \rangle = \langle \psi_A^\dagger \psi_A \rangle - \langle \psi_B^\dagger \psi_B \rangle \neq 0$  which describes charge density modulation between the two sub-lattices [15]. In Fig. 4 we plot  $\chi_z(l)$  within the perturbatively accessible parameter regime when the system flows towards the 1D limit, and  $\alpha_x$  is finite. In this case  $\chi_z$  diverges logarithmically:

$$\chi_z(l) \sim [\alpha_x(l)/\pi] \ln(4/[1 + \delta(l)]), \quad 1 + \delta(l) \rightarrow 0. \quad (12)$$

One can estimate the transition temperature  $T_c$  from the formula  $l^* = \ln(v_x \Lambda / T_c)$ , which gives for example (see Fig. 4):  $T_c \approx 2\text{K}$  ( $l^* \approx 10.3$ ),  $T_c \approx 45\text{K}$  ( $l^* \approx 7$ ),  $T_c \approx 5 \times 10^3\text{K}$  ( $l^* \approx 2.2$ ). Naturally  $T_c$  increases with increasing  $\alpha_x$ .

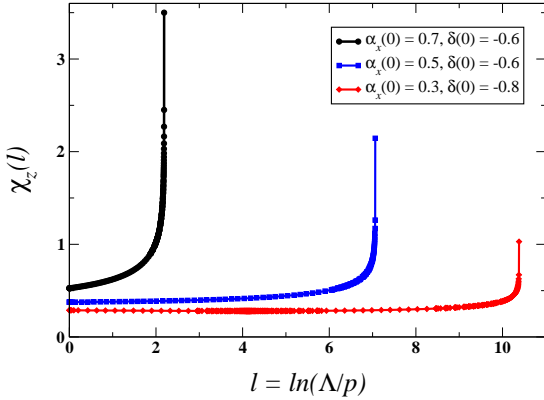


FIG. 4: (Color online) Dominant divergent susceptibility  $\chi_z(l)$  corresponding to the order parameter  $\langle \Psi^\dagger \hat{\sigma}_z \Psi \rangle$ , for different initial couplings ( $\alpha_x > \alpha_{x,c}(\delta)$ ). The divergence is at  $l = l^*$  where the system approaches the 1D limit,  $\delta(l) \rightarrow -1$ .

From Eq. (11) we find numerically that  $\chi_y$  also diverges in the 1D limit, but is always smaller than  $\chi_z$ , meaning that nematic-type (gapless) order is competing in the ground state. It is interesting to note that in studies of sliding Luttinger liquid (SLL) phases [18] one typically finds smectic non-Fermi liquid metals as well as charge ordered states. Notice that the irrelevance of the inter-chain hopping (our  $v_y$ ) is one of the main characteristics of the SLL. Our analysis is valid, strictly speaking, for

weak coupling while non-perturbative methods (such as excitonic pairing equations as well as bosonization) are needed to further quantify the exact shape of the phase boundary in the strong coupling regime ( $\alpha_x \sim 1$ ). However the overall topology of the phase boundary as well as the quantitative behavior at small  $\alpha_x$  are well captured within our approach.

Finally, in the weak coupling region  $\alpha_x < 0.5$  we find that the renormalization factor  $Z$  decreases as the system approaches 1D. From Eq. (4) we obtain  $\frac{dZ}{dt} = -\frac{Z\alpha_x^2}{6(1+\delta)}$ , which leads to the following behavior near the 1D line:

$$Z(l) \sim (1 + \delta(l))^{1/4}, \quad 1 + \delta(l) \rightarrow 0. \quad (13)$$

Notice that  $Z$  vanishes with a universal exponent 1/4, independent of the interaction  $\alpha_x$ .

*Summary and outlook.* In conclusion, we have found that the interplay between the anisotropy of the Dirac spectrum and long-range electron-electron interactions can lead to rich variety of behavior and two main electronic regimes: (i) a weak coupling phase characterized by a flow toward isotropic Dirac physics but with strongly renormalized parameters at low energies, and (ii) a quasi one-dimensional phase with dominant charge density wave order (anisotropic excitonic insulator). The strong anisotropic tendencies can manifest themselves in a variety of ways, such as squeezing of the Landau level spectrum in magnetic field [19], increase of the density of states which would favor itinerant ferromagnetism and affect (increase) the specific heat [11], and strong anisotropies in transport [6]. The value of the interaction on typical substrates is  $\alpha \approx 0.5 - 0.9$  [11], while strain of about 15% in the zig-zag direction leads to anisotropy  $|\delta| \approx 1/2$  [6], sufficient to push graphene into the anisotropic regime. We also expect that artificially engineered graphene (optical lattices and molecular graphene [10]) can provide a promising way to investigate the strongly anisotropic states found in the present work.

*Acknowledgments.* We are grateful to V.M. Pereira, E. Fradkin, B. Uchoa, F. Guinea, M. Vozmediano, O. Vafek, H. Fertig, A. Del Maestro, and A.V. Chubukov for stimulating discussions and comments. This work was supported by DOE grant DE-FG02-08ER46512.

- 
- [1] K. S. Novoselov *et al.*, Science **306**, 666 (2004).
  - [2] C. Lee *et al.*, Science **321**, 385 (2008).
  - [3] A. A. Balandin *et al.*, Nano Lett. **8**, 902 (2008).
  - [4] A. H. Castro Neto *et al.*, Rev. Mod. Phys. **81**, 109 (2009).
  - [5] N. M. R. Peres, Rev. Mod. Phys. **82**, 2673 (2010); S. Das Sarma *et al.*, Rev. Mod. Phys. **83**, 407 (2011).
  - [6] V. M. Pereira, A. H. Castro Neto, and N. M. R. Peres, Phys. Rev. B **80**, 045401 (2009); R. M. Ribeiro *et al.*, New J. Phys. **11**, 115002 (2009); M. O. Goerbig *et al.*

- Phys. Rev. B **78**, 045415 (2008); S. -M. Choi, S. -H. Jhi, and Y. -W. Son, Phys. Rev. B **81**, 081407(R) (2010).
- [7] C. -H. Park *et al.*, Nature Physics **4**, 213 (2008); S. Rusponi *et al.*, Phys. Rev. Lett. **105**, 246803 (2010);
- [8] V. M. Pereira, and A. H. Castro Neto, Phys. Rev. Lett. **103**, 046801 (2009). V. M. Pereira *et al.*, Europhys. Lett. **92**, 67001 (2010); O. Bahat-Treidel *et al.*, Phys. Rev. Lett. **104**, 063901 (2010); F. M. D. Pellegrino, G. G. N. Angilella, and R. Pucci, Phys. Rev. B **84**, 195404 (2011).
- [9] C. -Y. Moon *et al.*, Phys. Rev. B **84**, 195425 (2011); F. Virot *et al.*, Phys. Rev. Lett. **106**, 236806 (2011); S. Tang and M. S. Dresselhaus, Nano Lett. **12**, 2021 (2012).
- [10] L. Tarruell *et al.*, Nature **483**, 302 (2012); K. K. Gomes *et al.*, Nature **483**, 306 (2012).
- [11] For a review, see V. N. Kotov *et al.*, Rev. Mod. Phys. **84**, 1067 (2012).
- [12] D. C. Elias *et al.*, Nature Physics **7**, 701 (2011).
- [13] O. Vafek, Z. Tešanović, and M. Franz, Phys. Rev. Lett. **89**, 157003 (2001); D. J. Lee and I. F. Herbut, Phys. Rev. B **66**, 094512 (2002).
- [14] E. -A. Kim *et al.*, Phys. Rev. B **77**, 184514 (2008); Y. Huh and S. Sachdev, Phys. Rev. B **78**, 064512 (2008).
- [15] D. V. Khveshchenko, J. Phys.: Condens. Matter **21**, 075303 (2009), and cited references; E. Drut and T. A. Lahde, Phys. Rev. Lett. **102**, 026802 (2009); O. V. Gamayun, E. V. Gorbar, and V. P. Gusynin, Phys. Rev. B **81**, 075429 (2010).
- [16] O. Vafek and M. J. Case, Phys. Rev. B **77**, 033410 (2008); E. G. Mishchenko, Phys. Rev. Lett. **98**, 216801 (2007); V. N. Kotov, B. Uchoa, and A. H. Castro Neto, Phys. Rev. B **78**, 035119 (2008).
- [17] A. V. Chubukov, Physica C **469**, 640 (2009); O. Vafek and K. Yang, Phys. Rev. B **81**, 041401(R) (2010).
- [18] V. J. Emery *et al.*, Phys. Rev. Lett. **85**, 2160 (2000); A. Vishwanath and D. Carpentier, Phys. Rev. Lett. **86**, 676 (2001); R. Mukhopadhyay, C. L. Kane, and T. C. Lubensky, Phys. Rev. B **64**, 045120 (2001).
- [19] M. O. Goerbig, Rev. Mod. Phys. **83**, 1193 (2011).